# Microdisk Electrode Voltammetry: Theoretical Characterization and Experimental Verification of a Novel Electrocatalytic Mechanism

**Benjamin A. Brookes, Nathan S. Lawrence, and Richard G. Compton\***

*Physical and Theoretical Chemistry Laboratory, Oxford University, South Parks Road, Oxford, OX1 3QZ, United Kingdom*

A numerical method is used to characterize the steady-state voltammetry at microdisk electrodes of a new electrocatalytic reaction. This reaction, which occurs for the oxidation of *N*,*N*-dimethylphenylenediamine (DMPD, A) in the presence of $H_2S$ (X) is believed to proceed via the following route: $A - 2e^- \rightleftarrows B$, $B + X \rightarrow B-X$ ($k_2$), $B-X - 2e^- \rightleftarrows [B-X]^{2+}$. Due to the presence of a reagent restricted homogeneous kinetic step, the reaction is labeled $EC_{2X}E$. The numerical method for simulating this reaction scheme is based on the finite-difference formulation of coupled mass transport and kinetic equations in oblate spherical coordinates. The method is illustrated for not only the $EC_{2X}E$ but also the EC' reaction and is applicable to the simulation of steady-state limiting currents at microdisk electrodes. Iterative solutions are calculated using a Gauss−Newton scheme to overcome nonlinear homogeneous kinetic terms. The spatial convergence of the simulation for both reactions is investigated by considering the form of the concentration function describing the species. Via the comparison of working surfaces generated from simulated results, measuring the steady-state limiting current is shown to be insensitive to the resolution of EC', ECE, and $EC_{2X}E$ reactions. Experimental steady-state limiting current data is reported for the DMPD/$H_2S$ system at microelectrodes of 7.3, 19.5, and 25.0 $\mu$m diameter to verify the theory behind the $EC_{2X}E$ reaction. These results are shown to closely fit experimental data using a working surface interpolation method. Specifically, this method correctly predicts the variation of the steady-state limiting current with the concentration of $H_2S$ for a 19.5 $\mu$m diameter microelectrode to a relative standard deviation of 1.9%. Similar analysis for the 7.3 and 25.0 $\mu$m electrodes results in a mean value of $1.4 \times 10^7$ mol$^{-1}$ cm$^3$ s$^{-1}$ for the rate constant $k_2$ in the DMPD/$H_2S$ system.

## Introduction

The flexibility of microdisk electrodes to interrogate fast electrochemical reactions has resulted in a wide range of analytical,[1−6] semianalytical[7,8] and numerical methods to solve many predominantly first-order mechanisms (E, CE, EC, EC', ECE, DISP1, DISP2, and $EC_2E$). Simulations using finite difference[9−18] and finite element[19−22] methods have received much attention in previous literature due to the problem of achieving efficient convergence as a result of the flux singularity at the electrode edge. Early finite difference methods for solving such a system involved transient simulations using either fully explicit Hopscotch[9,13] or semiexplicit (ADI[12]) algorithms, and solving to a converged result. It is possible to use successive overrelaxation methods[23] (SOR) or ADI to solve directly to steady state. However, fully implicit direct steady-state solution methods, such as the strongly implicit procedure[24,25] (SIP) and Multigrid[26,27] methods have been shown to be more efficient. Even so, these methods are limited by their inability to cope with implicit kinetic schemes, often necessary for convergence when simulating complex reactions. For these coupled schemes, direct matrix methods, such as the preconditioned Krylov subspace (PKS) methods,[15] rather than stencil-based solvers, have been shown to be flexible for solving complex reactions, since different sparsity patterns may be accommodated. While the problem of the edge singularity has been circumvented by several different techniques, detailed in work by Harrimann et
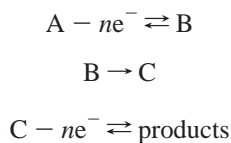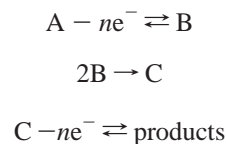
al.,[20] the use of a conformal map proves one of the easier methods for accurate simulation of coupled reactions. Two conformal maps for the microdisk electrode, the first by Amatore and Fosset[17] and the second by Verbrugge and Baker,[18] (both of which are derived from Michael's oblate spherical coordinates[9]) result in closed-space simulations, and remove the discontinuous boundary condition between the electrode surface and insulating wall. Alden[28] has shown the solution of mass transport equations under the Amatore transformation the more efficient of the two for simulating a variety of predominantly first-order reaction mechanisms under steady state conditions. This can be mainly attributed to the fact that the diffusion-only mass transport is a plane in the $\Gamma$ coordinate and hence can be solved on relatively coarse grids.

The particular problem we address in this paper is one that has recently arisen in the electrochemical detection of $H_2S$ using *N*,*N*-dimethylphenylenediamine (DMPD, NH$_2$C$_6$H$_4$NMe$_2$) as a redox mediator.[29] This is thought to proceed via the following route:

$$A - 2e^- \rightleftarrows B$$

$$B + X \rightarrow B-X$$

$$B-X - 2e^- \rightleftarrows [B-X]^{2+}$$
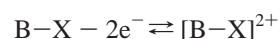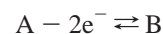
where A = DMPD and X = $H_2S$. The reaction is similar to, but distinct from, the familiar ECE

Microdisk Electrode Voltammetry

*J. Phys. Chem. B, Vol. 104, No. 47, 2000* **11259**

$$A - ne^- \rightleftarrows B$$

$$B \rightarrow C$$

$$C - ne^- \rightleftarrows products$$

EC$_2$E

$$A - ne^- \rightleftarrows B$$

$$2B \rightarrow C$$

$$C - ne^- \rightleftarrows products$$

and EC′ reactions

$$A - ne^- \rightleftarrows B$$

$$B + X \rightarrow A + products$$
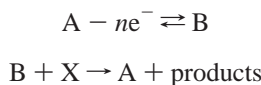
In particular, we illustrate when the concentration of X is low, the mechanistic distinction from the EC′ reaction via limiting current analysis alone is unlikely to be experimentally viable. Accordingly, in this paper we develop the voltammetric theory for the new reaction type, which we label EC$_{2X}$E to emphasize both the similarity with the ECE pathways and the second order nature of the coupled chemical step. Specifically, we solve the limiting current problem for the EC$_{2X}$E and for comparison the EC′ mechanism at microdisk electrodes, noting that the full kinetic pathway of the DMPD/H$_2$S reaction has been accomplished with independent methods. Further, comparison is made with experimental data obtained for this system.

Since we seek a single method that will be able to applicable to both the EC$_{2X}$E and EC′ mechanisms, we attempt to solve the EC$_{2X}$E problem using the same fully-implicit linearization method as implemented by Alden[15] in the "sparse matrix approach" and, for ease of computation, solve a banded matrix equation. Although we do not make use of the memory-efficient sparse matrix methods, the coding of such a method proves relatively facile. Also, the inclusion of implicit homogeneous kinetics is expected to lead to fast convergence, even at fast kinetic limits.

**Theory**

The mass transport of a species A to a microdisk electrode is given in Cartesian coordinates by

$$\frac{\partial a}{\partial t} = D_A \left\{ \frac{\partial^2 a}{\partial z^2} + \frac{\partial^2 a}{\partial r^2} + \frac{1}{r}\frac{\partial a}{\partial r} \right\} \tag{1}$$

where $a = [A]/[A]_{bulk}$, $D_A$ is the diffusion coefficient of A, $z$ is the distance normal to the electrode, and $r$ is the radial coordinate.

Equation 1 may be written in dimensionless form as

$$\frac{\partial a}{\partial \tau} = \frac{\partial^2 a}{\partial Z^2} + \frac{\partial^2 a}{\partial R^2} + \frac{1}{R}\frac{\partial a}{\partial R} \tag{2}$$

where $\tau = tD_A/r_e^2$, $R = r/r_e$, $Z = z/r_e$, and $r_e$ is the radius of the electrode.

The Amatore and Fosset[17] transformation demands the following change of variables:

$$Z = \theta \tan(^1/_2\pi\Gamma), \quad R = \frac{\sqrt{1 - \theta^2}}{\cos(^1/_2\pi\Gamma)}$$

**TABLE 1: Boundary Conditions for the Mass Transport Equations Which Describe the EC$_{2X}$E and EC′ Reactions**

| $\Gamma$ | $\theta$ | EC$_{2X}$E | EC′ |
|---|---|---|---|
| 0 | all | $a = 0$, $\partial b/\partial\Gamma = 0$, $c = 0$, $\partial x/\partial\Gamma = 0$ | $\partial a/\partial\Gamma = \partial b/\partial\Gamma$, $\partial x/\partial\Gamma = 0$ |
| 1 | all | $a = 1$, $b = 0$, $c = 0$, $x = \gamma$ | $a = 1$, $b = 0$, $x = \gamma$ |
| all | 1,0 | $\partial a/\partial\Gamma = \partial b/\partial\Gamma$, $\partial c/\partial\Gamma = \partial x/\partial\Gamma = 0$ | $\partial a/\partial\Gamma = \partial b/\partial\Gamma = \partial c/\partial\Gamma = \partial x/\partial\Gamma = 0$ |

$\Gamma$ is the transformed radial distance, ranging from 0 to 1, corresponding to real distances of 0 and infinity. $\theta$ is the transformed angular component sweeping between normal to the electrode ($\theta = 0$) and parallel to the electrode ($\theta = 1$).

Mass transport eq 2 becomes

$$\frac{\partial a}{\partial \tau} = \frac{1}{[\theta^2 + \tan^2(^\pi/_2\Gamma)]}\left\{\frac{4}{\pi^2}\cos^2(^\pi/_2\Gamma)\frac{\partial^2 a}{\partial\Gamma^2} + \frac{\partial}{\partial\theta}\left[(1 - \theta^2)\frac{\partial a}{\partial\theta}\right]\right\} = \nabla(\Gamma,\theta)^2 a \tag{3}$$

The dimensionless current, $\psi$, is given by

$$\psi = \int_0^1 \frac{\partial a}{\partial\Gamma}|_{\Gamma=0}\, d\theta \tag{4}$$

and the observed current, $I$, by

$$I = 4\pi r_e FD_a \int_0^1 \frac{\partial a}{\partial\Gamma}|_{\Gamma=0}\, d\theta \tag{5}$$

Assuming that $D_A = D_B = D_C \neq D_X$, the full set of mass transport equations for the EC$_{2X}$E reaction, at steady state, is

$$\frac{\partial a}{\partial \tau} = \nabla(\Gamma,\theta)^2 a = 0 \tag{6a}$$

$$\frac{\partial b}{\partial \tau} = \nabla(\Gamma,\theta)^2 b - k_{norm}bx = 0 \tag{6b}$$

$$\frac{\partial x}{\partial \tau} = \kappa_x\nabla(\Gamma,\theta)^2 x - k_{norm}bx = 0 \tag{6c}$$

$$\frac{\partial c}{\partial \tau} = \nabla(\Gamma,\theta)^2 c + k_{norm}bx = 0 \tag{6d}$$

where $\kappa_x = D_X/D_A$ and $k_{norm} = k_2[A]_{bulk}\, r_e^2/D_A$. Mass transport equations for the EC′ reaction are

$$\frac{\partial a}{\partial \tau} = \nabla(\Gamma,\theta)^2 a + k_{norm}bx = 0 \tag{6e}$$

$$\frac{\partial b}{\partial \tau} = \nabla(\Gamma,\theta)^2 b - k_{norm}bx = 0 \tag{6f}$$

$$\frac{\partial x}{\partial \tau} = \kappa_x\nabla(\Gamma,\theta)^2 x - k_{norm}bx = 0 \tag{6g}$$

The assumption that all electroactive species are completely destroyed at the electrode surface results in the boundary conditions given in Table 1. In the EC$_{2X}$E reaction under steady-state conditions, the solution of eq 4a is

$$a(\theta,\Gamma) = \Gamma \tag{7}$$

since species A undergoes no homogeneous kinetics. The mass transport problem for B can thus be solved without simulating species A, and the EC$_{2X}$E reaction therefore becomes a coupled three species problem. The EC′ reaction has already been solved

by Tutty,[30] who has shown that the mass transport equations for species A and B reduce to a single PDE:

$$\nabla(\theta,\Gamma)^2(D_A a + D_B b) = 0 \qquad (8)$$

which possesses the solution

$$D_A a + D_B b = D_A \qquad (9)$$

within the specified boundary conditions for species A and B. Substitution of eq 6 into eqs 4e–g eliminates one PDE. This is not possible for the EC$_{2X}$E reaction due to the mixed Dirichlet and Neumann boundary conditions for B, X, and C at the electrode surface and at the diffusion layer. However, for the purposes of consistency in the method developed in this paper, we will demonstrate the solution of mass transport eqs 4e–f by considering it as a three species problem and using the same banded matrix approach as the EC$_{2X}$E reaction.

Since the $\theta$ and $\Gamma$ coordinates both range between 0 and 1, we define a regular square grid of size $N_J \times N_K$ nodes, such that $^S u_{j,k}$ is the approximate solution to the concentration of species a S at the location

$$\theta = k\Delta\theta \quad (1 \le k \le N_K) \qquad (10)$$

$$\Gamma = j\Delta\Gamma \quad (1 \le j \le N_J) \qquad (11)$$

where

$$\Delta\Gamma = \frac{1}{N_J + 1} \qquad \Delta\theta = \frac{1}{N_K + 1} \qquad (12)$$

We now discretize the set of partial differential equation in the grid domain using the central difference equations:

$$\left(\frac{\partial^2 u}{\partial\Gamma^2}\right)_{j,k} \approx \frac{u_{j+1,k} - 2u_{j,k} + u_{j-1,k}}{(\Delta\Gamma)^2} \qquad (13)$$

$$\left(\frac{\partial^2 u}{\partial\theta^2}\right)_{j,k} \approx \frac{u_{j,k+1} - 2u_{j,k} + u_{j,k-1}}{(\Delta\theta)^2} \qquad (14)$$

$$\left(\frac{\partial u}{\partial\theta}\right)_{j,k} \approx \frac{u_{j,k+1} + u_{j,k-1}}{2\Delta\Gamma} \qquad (15)$$

The implementation of the finite difference equations results in the mass transport equations, for any species, S, becoming

$$0 = (\lambda_{\theta d} - \lambda_{\theta s})^S u_{j,k-1} + (\lambda_{\Gamma d})^S u_{j-1,k} + (-2\lambda_{\Gamma d} - 2\lambda_{\theta d})^S u_{j,k} +$$
$$(\lambda_{\Gamma d})^S u_{j,k+1} + (\lambda_{\theta d} + \lambda_{\theta s})^S u_{j+1,k} \pm k_{\text{norm}}\,{}^{S'} u_{j,k}\,{}^{S''} u_{j,k} \qquad (16)$$

where

$$\lambda_{\Gamma d} = \frac{4\omega\cos^2(^1/_2\pi\Gamma)}{\pi^2(\Delta\Gamma)^2}$$

$$\lambda_{\theta d} = \frac{\omega(1 - \theta^2)}{(\Delta\theta)^2}$$

$$\lambda_{\theta s} = \frac{-\omega\theta}{\Delta\theta}$$

$$\omega = [\theta^2 + \tan^2(^1/_2\pi\Gamma)]^{-1}, \quad \Delta\theta = [NK - 1]^{-1},$$
$$\Delta\Gamma = [NJ - 1]^{-1}$$

Note that species S′ and S″ may or may not be the same as species S. In the EC$_{2X}$E reaction, we define the vector $\mathbf{u}_{j,k}$ as

$$\mathbf{u}_{j,k} = \begin{bmatrix} b_{j,k} \\ x_{j,k} \\ c_{j,k} \end{bmatrix}$$

For the EC′ reaction, species C is replaced by A, so that Also

$$\mathbf{u}_{j,k} = \begin{bmatrix} b_{j,k} \\ x_{j,k} \\ a_{j,k} \end{bmatrix}$$

defining the following $3 \times 3$ matrices

$$\mathbf{a}_{j,k} = \begin{bmatrix} \lambda_{\Gamma d} & 0 & 0 \\ 0 & \kappa_x\lambda_{\Gamma d} & 0 \\ 0 & 0 & \lambda_{\Gamma d} \end{bmatrix}$$

$$\mathbf{b}_{j,k} = \begin{bmatrix} \lambda_{\theta d} - \lambda_{\theta s} & 0 & 0 \\ 0 & \kappa_x(\lambda_{\theta d} - \lambda_{\theta s}) & 0 \\ 0 & 0 & \lambda_{\theta d} - \lambda_{\theta s} \end{bmatrix}$$

$$\mathbf{c}_{j,k} = \begin{bmatrix} -2\lambda_{\theta d} -2\lambda_{\Gamma d} & 0 & 0 \\ 0 & \kappa_x(-2\lambda_{\theta d} - 2\lambda_{\Gamma s}) & 0 \\ 0 & 0 & -2\lambda_{\theta d} - 2\lambda_{\Gamma d} \end{bmatrix}$$

$$\mathbf{d}_{j,k} = \begin{bmatrix} \lambda_{\theta d} + \lambda_{\theta s} & 0 & 0 \\ 0 & \kappa_x(\lambda_{\theta d} + \lambda_{\theta s}) & 0 \\ 0 & 0 & \lambda_{\theta d} + \lambda_{\theta s} \end{bmatrix}$$

$$\mathbf{e}_{j,k} = \begin{bmatrix} \lambda_{\Gamma d} & 0 & 0 \\ 0 & \kappa_x\lambda_{\Gamma d} & 0 \\ 0 & 0 & \lambda_{\Gamma d} \end{bmatrix}$$

the mass transport equations may be written as a matrix-vector equation to incorporate all three species at a given $j, k$ node:

$$\mathbf{q}_{j,k} = \mathbf{a}_{j,k}u_{j,k-1} + \mathbf{b}_{j,k}u_{j-1,k} + \mathbf{c}_{j,k}u_{j,k} + \mathbf{d}_{j,k}u_{j,k+1} + \mathbf{e}_{j,k}u_{j+1,k} +$$
$$\hat{N}(u_{j,k}) \quad (17)$$

where $\hat{N}$ is a nonlinear kinetic operator matrix of size $3 \times 3$, such that

$$\hat{N}(\mathbf{u}_{j,k}) = \begin{bmatrix} -k_{\text{norm}}b_{j,k}x_{j,k} \\ -k_{\text{norm}}b_{j,k}x_{j,k} \\ -k_{\text{norm}}b_{j,k}x_{j,k} \end{bmatrix}$$

and

$$\mathbf{q}_{j,k} = \begin{pmatrix} 0 \\ 0 \\ 0 \end{pmatrix}$$

since we are at steady state.

This mapping ensures that the bandwidth of the final matrix is minimized. We want to linearize the nonlinear matrix $\hat{N}(\mathbf{u})$, to obtain a linear $3\times3$ matrix operator, $\hat{\ell}$ that approximates $\hat{N}$, so we have

$$q_{j,k} = \mathbf{a}_{j,k}u_{j,k-1} + \mathbf{b}_{j,k}u_{j-1,k} + \mathbf{c}_{j,k}u_{j,k} + \mathbf{d}_{j,k}u_{j,k+1} + \mathbf{e}_{j,k}u_{j+1,k} +$$
$$\hat{\ell}_{j,k}(u_{j,k}) \quad (18)$$

For the $n + 1$th iterate, to a first-order approximation in a Taylor expansion

Microdisk Electrode Voltammetry

*J. Phys. Chem. B, Vol. 104, No. 47, 2000* **11261**

$$\hat{\mathbf{N}}(\mathbf{u}_{j,k}^{n+1}) = \hat{\mathbf{N}}(\mathbf{u}_{j,k}^{n}) - \mathbf{J}_{j,k}^{n}[\hat{\mathbf{N}}(\mathbf{u}_{j,k}^{n})][\mathbf{u}_{j,k}^{n} - \mathbf{u}_{j,k}^{n+1}] \equiv$$

$$\frac{\ell}{j,k}(\mathbf{u}_{j,k}^{n}) \quad (19)$$

where $\mathbf{J}_{j,k}^{n}[\hat{\mathbf{N}}(\mathbf{u}_{j,k}^{n})]$ is the Jacobian matrix of $\hat{\mathbf{N}}(\mathbf{u}_{j,k}^{n})$ evaluated at the $n$th iteration. The general form of $\mathbf{J}_{j,k}^{n}[\hat{\mathbf{N}}(\mathbf{u}_{j,k}^{n})]$ for both the EC$_2$XE and EC′ systems is

$$\mathbf{J}_{j,k}^{n}[\hat{\mathbf{N}}(\mathbf{u}_{j,k})] = \begin{bmatrix} -k_{\text{norm}}x_{j,k}^{n} & -k_{\text{norm}}b_{j,k}^{n} & 0 \\ -k_{\text{norm}}x_{j,k}^{n} & -k_{\text{norm}}b_{j,k}^{n} & 0 \\ k_{\text{norm}}x_{j,k}^{n} & k_{\text{norm}}b_{j,k}^{n} & 0 \end{bmatrix}$$

and the term $\hat{\mathbf{N}}(\mathbf{u}_{j,k}^{n}) - \mathbf{J}_{j,k}^{n}[\hat{\mathbf{N}}(\mathbf{u}_{j,k})]\mathbf{u}_{j,k}$ becomes

$$\hat{\mathbf{N}}(\mathbf{u}_{j,k}^{n}) - \mathbf{J}_{j,k}^{n}[\hat{\mathbf{N}}(\mathbf{u}_{j,k}^{n})]\mathbf{u}_{j,k}^{n} = \begin{pmatrix} k_{\text{norm}}x_{j,k}^{n} \\ k_{\text{norm}}b_{j,k}^{n} \\ 0 \end{pmatrix}\mathbf{u}_{j,k}^{n} \quad (20)$$

We now extend the matrix eq 9, which is general for a point $j$, $k$, to all points on the grid. To do this, we build up vectors, indexing first by $k$ value and second by $j$ value, as defined below:

$$\mathbf{q}_j = \begin{pmatrix} \mathbf{q}_{j,1} \\ \mathbf{q}_{j,2} \\ \vdots \\ \mathbf{q}_{j,N_K-1} \\ \mathbf{q}_{j,N_K} \end{pmatrix} \in \mathbf{R}^{(3.N_K)}, \quad \mathbf{q} = \begin{pmatrix} \mathbf{q}_1 \\ \mathbf{q}_2 \\ \vdots \\ \mathbf{q}_{N_J-1} \\ \mathbf{q}_{N_J} \end{pmatrix} \in \mathbf{R}^{(3.N_K.N_J)}$$

$$\mathbf{u}_j = \begin{pmatrix} \mathbf{u}_{j,1} \\ \mathbf{u}_{j,2} \\ \vdots \\ \mathbf{u}_{j,N_J-1} \\ \mathbf{u}_{j,N_J} \end{pmatrix} \in \mathbf{R}^{(3.N_K)}, \quad \mathbf{u} = \begin{pmatrix} \mathbf{u}_1 \\ \mathbf{u}_2 \\ \vdots \\ \mathbf{u}_{N_J-1} \\ \mathbf{u}_{N_J} \end{pmatrix} \in \mathbf{R}^{(3.N_K.N_J)}$$

Equation 7 can now be rewritten as

$$\mathbf{M}\mathbf{u}^{n+1} - \mathbf{J}(\mathbf{u}^{n})\mathbf{u}^{n+1} = \mathbf{q} - \mathbf{J}(\mathbf{u}^{n})\mathbf{u}^{n} + \hat{\mathbf{N}}(\mathbf{u}^{n}) \quad (21)$$

where matrices $\mathbf{M}$ and $\mathbf{J}$ are formally defined as

$$\mathbf{M} = \begin{bmatrix} \mathbf{T}_1 & \mathbf{e}_1 & & & \\ \mathbf{a}_2 & \mathbf{T}_2 & \mathbf{e}_2 & & \\ & \mathbf{a}_3 & \vdots & \vdots & \\ & & \vdots & \mathbf{T}_{N_J-1} & \mathbf{e}_{N_J-1} \\ & & & \mathbf{a}_{N_J} & \mathbf{T}_{N_J} \end{bmatrix} \in \mathbf{R}^{(3.N_K.N_J)\times(3.N_K.N_J)}$$

$$\mathbf{J} = \begin{bmatrix} \mathbf{J}_1 & & & & \\ & \mathbf{J}_1 & & & \\ & & \vdots & & \\ & & & \mathbf{J}_{N_J-1} & \\ & & & & \mathbf{J}_{N_J} \end{bmatrix} \in \mathbf{R}^{(3.N_K.N_J)\times(3.N_K.N_J)}$$

and $\mathbf{T}_j$ is a tridiagonal matrix of the from

$$\mathbf{T}_j = \begin{bmatrix} \mathbf{c}_{j,1} + \mathbf{b}_{j,1} & \mathbf{d}_{j,1} & & & \\ \mathbf{b}_{J,2} & \mathbf{c}_{j,2} & \mathbf{d}_{j,2} & & \\ & \mathbf{b}_{j,3} & \vdots & \vdots & \\ & & \vdots & \mathbf{c}_{j,N_K-1} & \mathbf{d}_{j,N_K-1} \\ & & & \mathbf{b}_{j,N_K} & \mathbf{c}_{j,N_K} + \mathbf{d}_{j,N_K} \end{bmatrix} \in \mathbf{R}^{(3.N_K)^2}$$

and

$$\mathbf{a}_j = \begin{bmatrix} \mathbf{a}_{j,1} & & & & \\ & \mathbf{a}_{j,2} & & & \\ & & \vdots & & \\ & & & \mathbf{a}_{j,N_K-1} & \\ & & & & \mathbf{a}_{j,N_K} \end{bmatrix} \in \mathbf{R}^{(3.N_K)^2}$$

$$\mathbf{e}_j = \begin{bmatrix} \mathbf{e}_{j,1} & & & & \\ & \mathbf{e}_{j,2} & & & \\ & & \vdots & & \\ & & & \mathbf{e}_{j,N_K-1} & \\ & & & & \mathbf{e}_{j,N_K} \end{bmatrix} \in \mathbf{R}^{(3.N_K)^2}$$

$$\mathbf{J}_j = \begin{bmatrix} \mathbf{J}_{j,1} & & & & \\ & \mathbf{J}_{j,2} & & & \\ & & \vdots & & \\ & & & \mathbf{J}_{j,N_K-1} & \\ & & & & \mathbf{J}_{j,N_K} \end{bmatrix} \in \mathbf{R}^{(3.N_K)^2}$$

Note that the discretized no-flux boundary conditions at the extents of the $\theta$ domain as defined in Table 1 have already been imposed in matrix $\mathbf{T}_j$. Imposing the boundary conditions at the edges of the $\Gamma$ domain is more difficult since they differ for all species. For the EC$_2$XE reaction

$$\mathbf{c}_{1,k} = \begin{bmatrix} -2\lambda_{\Gamma d} & -\lambda_{\Gamma d} & 0 & 0 \\ 0 & -\kappa_x(\lambda_{\theta d} + \lambda_{\theta s}) & 0 \\ 0 & 0 & -2\lambda_{\theta d} & -2\lambda_{\Gamma d} \end{bmatrix}$$

$$\mathbf{q}_{1,k} = \begin{pmatrix} \lambda_{\Gamma d}\Delta\Gamma \\ 0 \\ 0 \end{pmatrix}$$

and

$$\mathbf{e}_{N_J,k} = 0, \quad \mathbf{q}_{N_J,k} = \begin{pmatrix} 0 \\ -\lambda_{\Gamma d}\gamma \\ 0 \end{pmatrix}$$

for all $k$.

For the EC′ reaction and

$$\mathbf{c}_{1,k} = \begin{bmatrix} -2\lambda_{\theta d} & -\lambda_{\Gamma d} & 0 & 0 \\ 0 & -\kappa_x(2\lambda_{\theta d} + \lambda_{\Gamma d}) & 0 \\ 0 & 0 & -2\lambda_{\theta d} & -2\lambda_{\Gamma d} \end{bmatrix}$$

$$\mathbf{e}_{N_J,k} = 0, \quad \mathbf{q}_{N_J,k} = \begin{pmatrix} 0 \\ -\lambda_{\Gamma d}\gamma \\ 0 \end{pmatrix}$$

for all $k$.

The overall sparsity pattern in matrix $\mathbf{M}$ is illustrated schematically in Figure 1a.

We define

$$\mathbf{M}^{n+1} = \mathbf{M}^{n} - \mathbf{J}[\hat{\mathbf{N}}(\mathbf{u}^{n})] \quad (22)$$

$$\mathbf{q}^{n+1} = \mathbf{q}^{n} - \mathbf{J}[\hat{\mathbf{N}}(\mathbf{u}^{n})] + \hat{\mathbf{N}}(\mathbf{u}^{n}) \quad (23)$$

So we now apply this Gauss−Newton iterative scheme to the problem

$$\mathbf{M}^{n+1}\mathbf{u}^{n+1} = \mathbf{q}^{n+1} \quad (24)$$

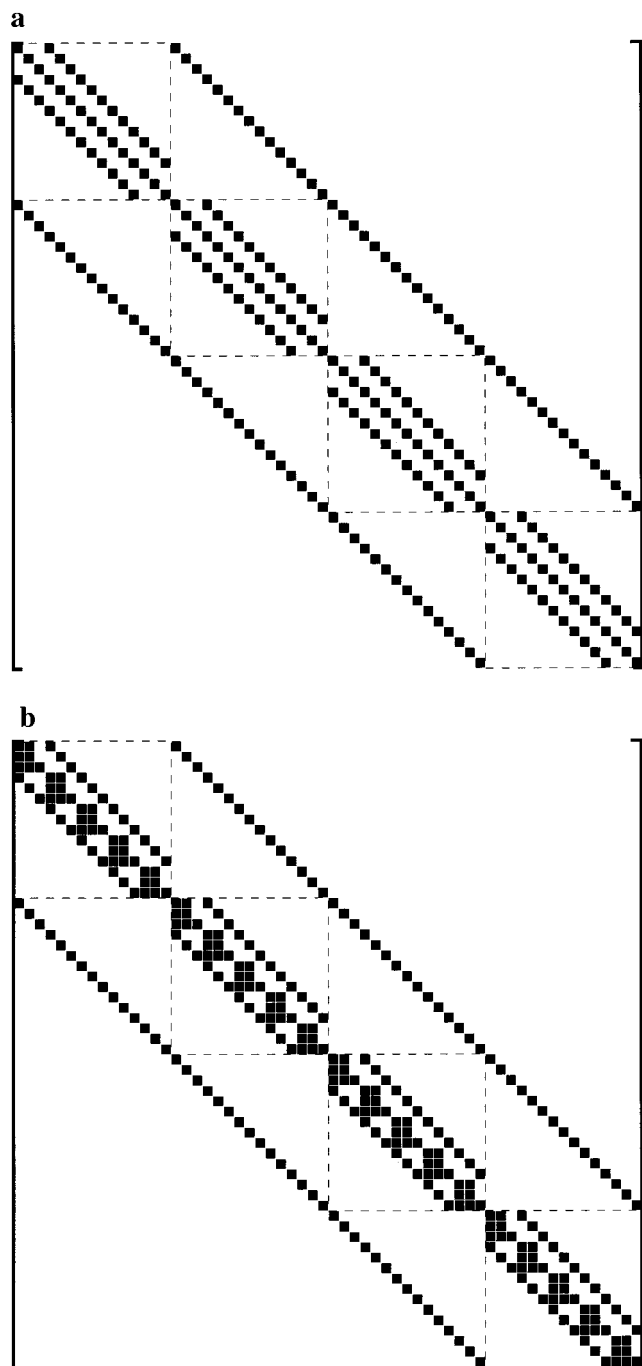until the current measured falls below a specified tolerance. The

**11262** *J. Phys. Chem. B, Vol. 104, No. 47, 2000*

Brookes et al.

**a**



**b**



**Figure 1.** Schematic diagram to illustrate the sparsity pattern of the matrix (a) $\mathbf{M}^n$ and (b) $\mathbf{M}^{n+1}$.

matrix eq 24 is solved using routines F07BDF and F07BEF of the NAG FORTRAN Subroutine Library.[31]

The sparsity pattern of the matrix $\mathbf{M}^{n+1}$ is illustrated in Figure 1b. The current for the species S is evaluated using trapezoidal quadrature and a 2-point flux approximation:

$$\psi_{\mathrm{S}} = \int_0^1 \frac{\partial u^{\mathrm{S}}}{\partial \Gamma}\Big|_{\Gamma=0}\, \mathrm{d}\theta \approx \frac{\Delta\theta}{\Delta\Gamma}\left[\frac{1}{2}u^{\mathrm{S}}_{1,0} + \sum_{k=1}^{NK} u^{\mathrm{S}}_{1,k} + \frac{1}{2}u^{\mathrm{S}}_{1,k+1}\right] \quad (25)$$

Substitution of the boundary condition at $\theta = 0$ and $\theta = 1$ gives

$$\psi_{\mathrm{S}} = \int_0^1 \frac{\partial u^{\mathrm{S}}}{\partial \Gamma}\Big|_{\Gamma=0}\, \mathrm{d}\theta \approx \frac{\Delta\theta}{\Delta\Gamma}\left[\frac{3}{2}u^{\mathrm{S}}_{1,1} + \sum_{k=2}^{NK-1} u^{\mathrm{S}}_{1,k} + \frac{3}{2}u^{\mathrm{S}}_{1,NK}\right] \quad (26)$$

Furthermore, we also consider the *effective number of electrons transferred*, $N_{\mathrm{eff}}$, which for the $\mathrm{EC_{2X}E}$ reaction is defined as

$$N_{\mathrm{eff}} = \psi_{\mathrm{A}} + \psi_{\mathrm{C}}$$

Since in this case, $\psi_{\mathrm{A}}$ for the steady-state limiting current reaction is unity, this reduces to

$$N_{\mathrm{eff}} = 1 + \psi_{\mathrm{C}}$$

For the EC′ reaction, $N_{\mathrm{eff}}$ is dependent on the current for the A species only, and is defined as

$$N_{\mathrm{eff}} = \psi_{\mathrm{A}}$$

where $\psi_{\mathrm{A}}$ is greater than unity when the value of $k_2$ is nonzero.

**Computing**. All simulations were written and compiled in FORTRAN 77 and run on a Silicon Graphics Origin 2000 server. Since the direct matrix method demands exceptionally large amounts of memory space, grids no larger than $50 \times 200$ were used (this alone requires 203 MB of memory to store the matrix in double precision floating point numbers). Data were analyzed using IDL 5.0

**Theoretical Results and Discussion**

First, the EC′ and $\mathrm{EC_{2X}E}$ reaction mechanisms are characterized, for the case where $D_x = D$. Later, we use the simulation to generate data under experimental conditions applicable to the DMPD/H$_2$S system at microdisk electrodes. The latter results are compared with those measured experimentally to validate the chemical reaction modeling.

**Convergence.** The convergence was considered for the case where $D_x = D$ and $\gamma = 1$. The presence of the linear approximation to the quadratic concentrations results in several iterates needing to be calculated before convergence in successive concentration vectors, $\tilde{\mathbf{u}}$, is achieved. Convergence was considered complete when the criterion

$$\mathrm{tol} = |\psi^n - \psi^{n+1}| < 10^{-5} \quad (27)$$

was achieved, where $\psi^n$ is the normalized current for the C species in the $\mathrm{EC_{2X}E}$ reaction, or the A species in the EC′ reaction. This typically occurred at $n = 6$ or $n = 7$ for high rate constants and for grids coarser than $50 \times 200$ nodes.

Figure 2, a and b, shows plots of the error in the steady-state value of $N_{\mathrm{eff}}$ calculated as

$$\mathrm{error} = \frac{N_{\mathrm{eff}}}{N_{\mathrm{eff}}^{50 \times 200}} - 1 \quad (28)$$

where $N_{\mathrm{eff}}^{50 \times 200}$ is the value given in a grid of $50 \times 200$ nodes,[18] for the $\mathrm{EC_{2X}E}$ mechanism and EC′ mechanism, respectively. Whereas in the $\mathrm{EC_{2X}E}$ reaction the error increases with increasing values of $k_{\mathrm{norm}}$, for the EC′ reaction, it remains small (less than 1% for a $15 \times 15$ grid) over the entire range of $k_2$ studied. Since convergence errors are attributable to the quality by which conformal map describes concentration distribution of the chemical species in space, we investigated the reason for the errors by considering first the dimensionless homogeneous chemical reaction rate, $K$, which we define as

$$K = k_{\mathrm{norm}} b x \quad (29)$$

and the second concentration profile of the C species in the $\mathrm{EC_{2X}E}$ reaction for $\gamma = 1$ and $\log(k_{\mathrm{norm}})$ ranging from 0 to 6. Figure 3 shows the form of the chemical activity, $K$, in $\Gamma$ and
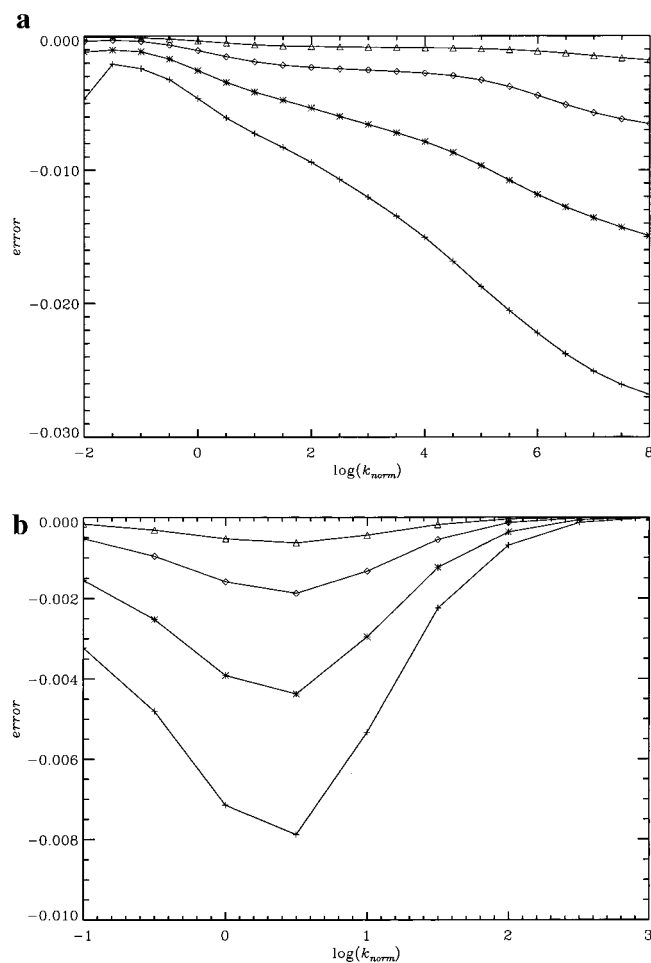
Microdisk Electrode Voltammetry

*J. Phys. Chem. B, Vol. 104, No. 47, 2000* **11263**

**a**



**b**



**Figure 2.** (a) Plot to show the error in the steady-state limiting current simulated on grids of sizes $15 \times 15$ (+), $25 \times 25$ (∗), $50 \times 50$ (◇), $50 \times 100$ (△) compared to a grid of $50 \times 200$ nodes for the $EC_{2X}E$ reaction. (b) Plot to show the error in the steady-state limiting current simulated on grid of sizes $15 \times 15$ (+), $25 \times 25$ (∗), $50 \times 50$ (◇), $50 \times 100$ (△) compared to a grid of $50 \times 200$ nodes for the EC′ reaction.

$\theta$ space and Figure 4 the concentration profiles of C. The noticeable trends as $k_{norm}$ increases are that the reaction zone, which may be defined as the area where $K$ is greater than some arbitrary fraction of its maximum value, decreases in size (moves to lower $\Gamma$ values). Also, the reaction zone becomes increasingly nonlinear in the $\theta$ coordinate, shifting toward the $\theta = 0$ axis and thus producing a local maximum around the electrode annulus. This can be attributed to an increase in the kinetic contribution to the mass transport which removes the $\theta$ invariance of the solution to the mass transport PDEs. The trends described above are mimicked by the form of the concentration of the C species, but in addition, there is a decrease in the total amount of the C species present in solution. This is a direct result of the reaction zone thinning, causing the C species to be generated closer to the electrode and hence more net consumption of C at the electrode occurs.

In kinetic limit, the reaction layer thins to the point were a singularity is produced in the concentration of the C species at the electrode surface. This results in a loss of accuracy in the 2-point flux calculation, which cannot be overcome by a higher order Taylor approximation.

In Figure 5, the concentration profile of the C species is plotted in Cartesian coordinates. This illustrates the difficulty in simulating the $EC_{2X}E$ mechanism without a conformal map. In diagrams 5c,d, this peak in concentration of the C species around the electrode annulus is shown to be considerably narrower in both the $R$ and $Z$ coordinates. This illustrates the complex nature of solving the $EC_{2X}E$ mechanism in Cartesian coordinates, even with efficient expanding grids.

In contrast to the $EC_{2X}E$ mechanism, in the EC′ reaction, as we move from $k_{norm} = 0$, to the kinetic limit of $k_{norm}$, reaction profile and the concentration distribution of the A species change from being at a maximum at the electrode surface, to the limit where the reaction layer stands off the electrode. This results in the concentration gradient of the A species at the electrode becoming more diffusion dominated, and therefore closer to a plane in $\Gamma$ space, thus maintaining high convergence. See ref 30 and references therein for a more complete description of the EC′ reaction at the microdisk electrode.

Working surface interpolation[33] has been shown as an excellent method for quantitative mechanistic interpolation. We use this method to first analyze differences in the theoretical results and latter for the analysis of experimental results. Consideration of the mass transport eqs 4a−g shows that the solution to $N_{eff}$ for the EC′ and the $EC_{2X}E$ reaction is a function of the following variables

$$N_{eff} = N_{eff}(k_{norm}, \gamma, \kappa_X) \qquad (30)$$

assuming that $D_a = D_b = D_c = D$. Thus specifying a set of diffusion coefficients leads to $N_{eff}$ being a sole function of $\gamma$ and $k_{norm}$, and it becomes possible to build up a working surface. We therefore investigate the similarities between the EC′ and the $EC_{2X}E$ reaction by generating working surfaces for both reactions with the test case, $\kappa_X = 1$. Simulations were accordingly run in the range $0 \leq \gamma \leq 1$ and $-4 \leq \log_{10}(K_{NORM}) \leq 8.0$. All simulations were performed on a grid of $N_K = 50$ by $N_J = 50$. Figure 6, a and b, shows the working surfaces for the $EC_{2X}E$ and EC′ reaction, respectively. Of particular note is that at both low and high $\gamma$ values, both working surfaces are difficult to distinguish. To investigate further, two working surfaces were generated (to form an $N \times N$ matrix of $N_{eff}$ values) which were then mapped onto each other by varying the value $\epsilon$, where $\epsilon = k_{norm}^{EC_{2X}E}/k_{norm}^{EC'}$, until the Frobenius norm of the difference between the two surfaces in the overlapping region was minimized. The Frobenius norm is defined as

$$||A-B||_F^2 = \sum_{i=1}^{N} \sum_{j=1}^{N} |(a_{ij} - b_{ij})|^2 \qquad (31)$$

where matrices $A$ and $B$ contain the working surface data for the EC′ and $EC_{2X}E$ reaction, respectively. The Frobenius norm was minimized at $\epsilon = 3.53$; the difference between the two working surfaces at this value is shown in Figure 7. The largest discrepancy between the surfaces occurs at the $\gamma$ value of 1.0, and at $\log(k_{norm})$ values of 1.76. From the general trend, it is evident that the discrepancy will increase with the $\gamma$ value, However, if as in the DMPD/H$_2$S system, where $\gamma$ is limited by solubility, investigating this domain may not be possible. This is because the EC′ mechanism regenerates species A therefore the concentration of X determines the kinetic limit of $N_{eff}$. In the $EC_{2X}E$ reaction, both X and B limits the generation of C, thus since B can never exceed the concentration of [A]$_{bulk}$, the kinetic limit of $N_{eff}$ is always 2.0. We should also note that in this kinetic limit of X → ∞, the $EC_{2X}E$ reaction is indistinguishable from the ECE reaction. To illustrate the similarity of the working curves for both reactions in the experimental domain, we define a new rate constant, $k'_{norm}$. For the $EC_{2X}E$ reaction
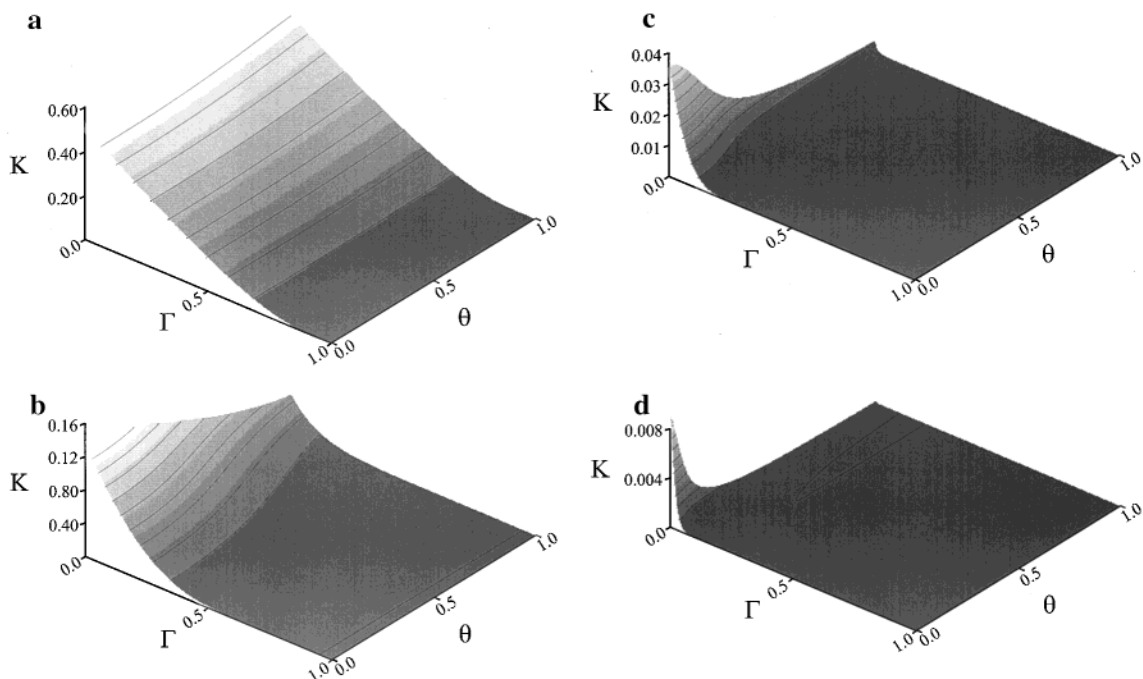
$$k'_{norm} = k_{norm}\gamma \qquad (32)$$

**Figure 3.** Plot showing the variation of the chemical activity, $K$, in $\Gamma$ and $\theta$ space for $\log(k_{norm}) =$ (a) 0, (b) 2, (c) 4, and (d) 6 in the $EC_{2X}E$ reaction.[23]
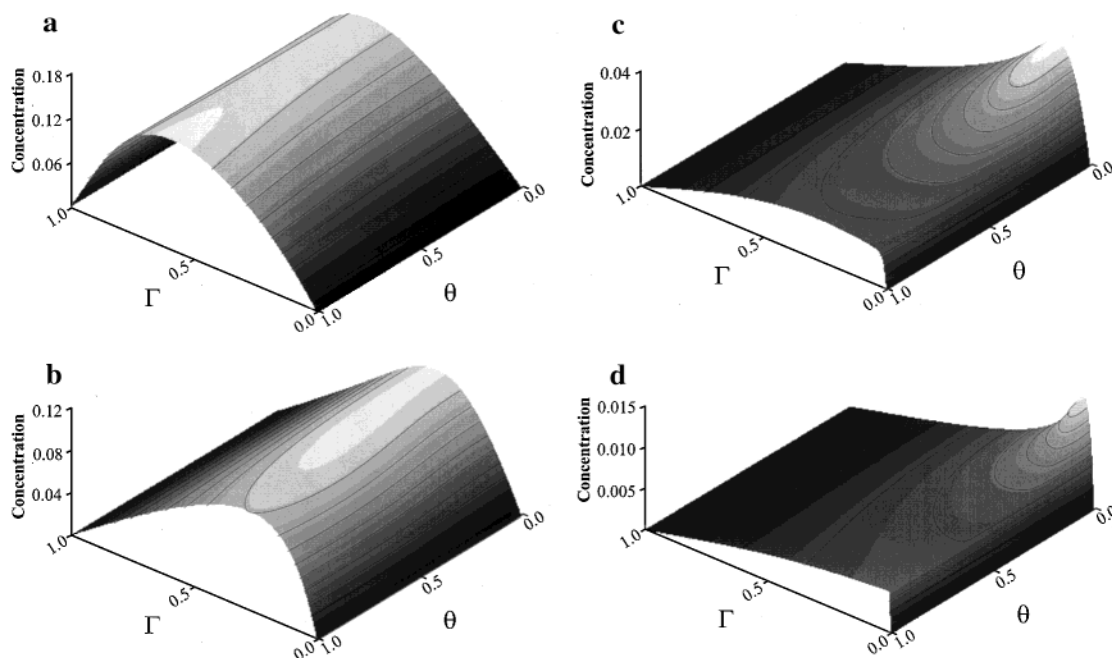


**Figure 4.** Plot showing the variation of the concentration of the species C, in $\Gamma$ and $\theta$ space and $\log(k_{norm}) =$ (a) 0, (b) 2, (c) 4, and (d) 6 in the $EC_{2X}E$ reaction. [37]

and for the ECE reaction

$$k'_{norm} = k_{ECE}[A]_{bulk} \, r_e^2/D_A \qquad (33)$$

where $k_{ECE}$ is the homogeneous rate constant. Figure 8 illustrates the similarity of working curve for the ECE reaction, with those for the $EC_{2X}E$ reaction. Of note is that at the value of $\gamma = 1$ the working curves for the ECE reaction and the $EC_{2X}E$ reaction differ by a maximum of 0.045 at $\log(k_{norm}) = -0.2$. This represents an error in the current of ca. 3%, which will commonly be less than experimental error, and hence alternative experimental techniques may be required to distinguish these reaction mechanisms.

Having analyzed the working surfaces for the case where $\kappa_X = 1$, we now consider using the working surface interpolation method as a way to quantitatively analyze mechanistic data from the DMPD/H$_2$S system.

**Experimental Section**

All reagents were obtained from Aldrich and were of the highest grade available and used without further purification. All solutions and subsequent dilutions were prepared using deionized water from an Elgastat (Elga, UK) UHQ grade water system with a resistivity of not less than 18 M$\Omega$ cm. Solutions were prepared by dissolving the appropriate analyte in pH 4 acetate buffer (0.1 M). In general, all the solutions were degassed
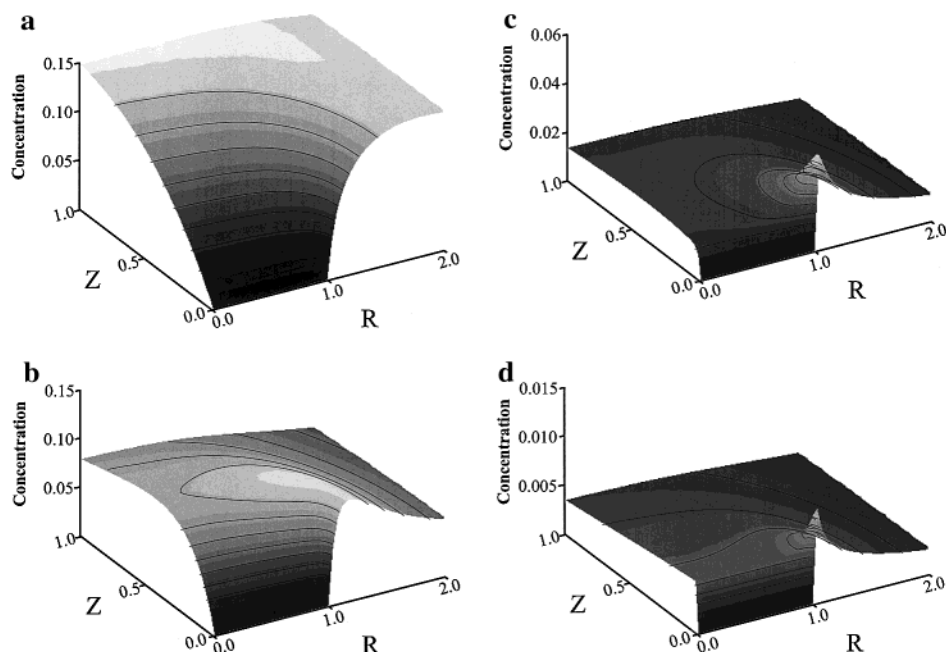
Microdisk Electrode Voltammetry

*J. Phys. Chem. B, Vol. 104, No. 47, 2000* **11265**



**Figure 5.** Plot showing the variation of the concentration of the species C, in Cartesian space for $\log(k_{norm})$ = (a) 0, (b) 2, (c) 4, and (d) 6 in the $EC_{2X}E$ reaction. [37]
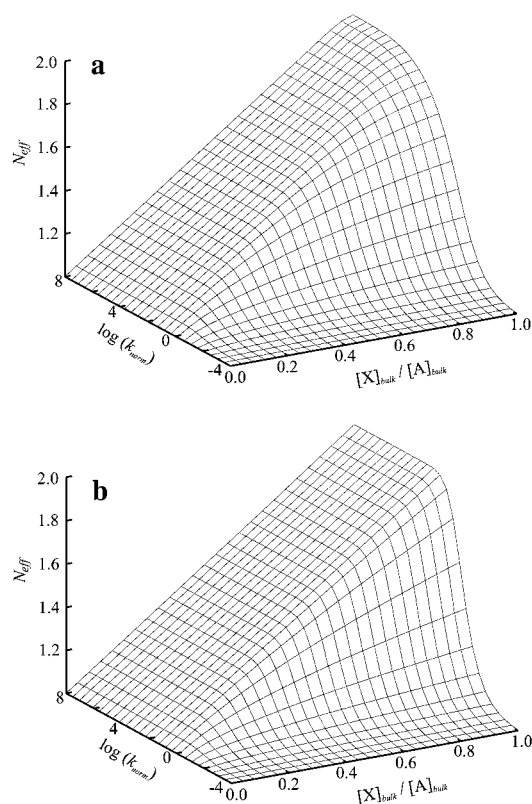


**Figure 6.** (a) Working surface for the $EC_{2X}E$ reaction ($\kappa_X = 1$). (b) Working surface for the $EC'$ reaction ($\kappa_X = 1$).



**Figure 7.** Plot showing the difference between the working surfaces of $EC_{2X}E$ and $EC'$ ($\kappa_X = 1$) reactions at $\epsilon = 3.53$.



**Figure 8.** Plot showing the working curves for the $EC_{2X}E$ reaction where $\kappa_X = 1$; $\gamma = 1$ ($\diamond$) and the ECE reaction where $\kappa_X = 1$ (+).

and stored under Argon with the DMPD being kept in the dark due to its photosensitivity. Stock sulfide solutions (0.05 M) were prepared by dissolving $Na_2S$ in previously degassed NaOH (25 mM) and were used within 1 h of preparation to minimize losses due to aerial oxidation.

Electrochemical measurements were recorded using an Autolab PGSTAT 30 computer controlled potentiostat (Eco-Chemie, Netherlands) with a standard three electrode configuration and a typical cell volume of 40 cm³. Two carbon and one platinum microdisk electrode (BAS Co., Ltd, Tokyo, Japan)
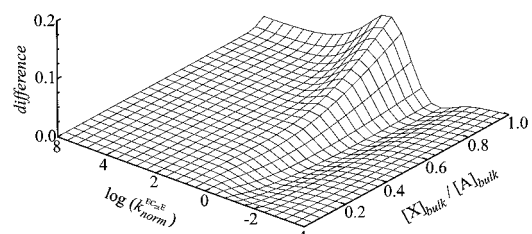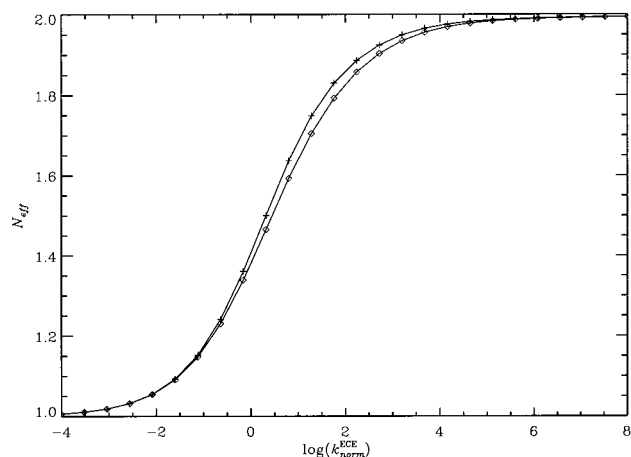
with nominal radii ranging from 3.5 to 12.5 $\mu$m served as the working electrode; platinum wire wound into a spiral provided the counter electrode and a saturated calomel reference electrode (SCE, Radiometer, Copenhagen) completed the cell assembly. The microelectrodes were carefully polished using 1.0 and 0.3 $\mu$m alumina (Buehler, USA)[20] before use. The microelectrodes were electrochemically calibrated prior to use to obtain an accurate measurement of electrode diameter. This was carried out in a solution containing 2.12 mM ferricyanide ($D = 0.76 \times 10^{-9}$ m² s⁻¹)[35] in 0.1 M aqueous KCl with linear sweep voltammograms (10 mV s⁻¹) recorded for each electrode. The

limiting currents were obtained and the corresponding electrode diameters were found to be $7.3 \pm 0.5$ and $19.5 \pm 0.5$ $\mu$m, respectively for the carbon electrodes, and $25.0 \pm 0.5$ $\mu$m for the platinum electrode.

Linear sweep voltammograms for the DMPD/H$_2$S system were recorded by scanning between 0V and +0.6 V. Where data for the limiting current variation as a function of sulfide concentration was necessary, voltammograms were sequentially scanned (starting with pure DMPD solution) after the addition of a known quantity of sufide solution.

### Results and Discussion

First the voltammetry of DMPD (186 $\mu$M, pH 4, $23 \pm 2$ °C) was studied at all three microdisk electrodes. In all cases, two nearly overlapping electrochemically reversible one electron waves were observed with $E_{1/2}$ = +0.28 V and +0.32 V vs SCE. The limiting current data was consistent with a diffusion coefficient of $9.7 \times 10^{-6}$ cm$^2$ s$^{-1}$; this compares favorably with the value of $(9 \pm 0.5) \times 10^{-6}$ cm$^2$ s$^{-1}$ deduced independently from cyclic voltammetric data.[29] Moreover, the limiting current increased with the introduction of sulfide (0−103 $\mu$M), which provides evidence for a coupled chemical reaction step, in which the oxidation product reacts with the H$_2$S forming further oxidizable products.

The well-established program DIGISIM[36] has been utilized previously[29] to model the cyclic voltammetry of the H$_2$S/DMPD system at a macroelectrode and gave evidence for the reaction pathway:

$$A - 2e^- \rightleftarrows B$$

$$B + X \xrightarrow{k_2} B-X$$

$$B-X - 2e^- \rightleftarrows [B-X]^{2+}$$
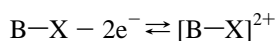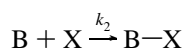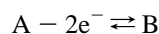
where A = DMPD and X = H$_2$S. Furthermore, the parameters which gave best agreement in the height for the second oxidation peak between the theoretical and experimental voltammograms were as follows: $D(\text{DMPDH}^+) = D(\text{DMPD}^{\bullet+}) = D(\text{DMPD}^+) = 9 \times 10^{-6}$ cm$^2$ s$^{-1}$, $D(\text{H}_2\text{S}) = 1.64 \times 10^{-5}$ cm$^2$ s$^{-1}$ and $k_2 = 8 \times 10^7$ mol$^{-1}$ cm$^3$ s$^{-1}$.

Experimental electrode limiting current data was collected for the DMPD/H$_2$S system at the microdisk electrodes of diameter 7.3, 19.5, and 25.0 $\mu$m, respectively. The concentration the DMPD solution and the range of concentration of H$_2$S in the electrolyte solution were identical to those detailed in the Experimental Section. $N_{\text{eff}}$ values were subsequently calculated as the ratio of the experimental limiting current to the current in the absence of redox mediation, that is, when the concentration of sulfide is zero.

To verify the theory behind the EC$_{2X}$E reaction, we use a working surface interpolation technique to analyze experimental data. This method involves the determination of an optimized rate constant, $k_{\text{norm}}^{\text{opt}}$, which best fits the experimental data. $N_{\text{eff}}$ data is used since this results in the removal of systematic errors in limiting currents. Computationally, $k_{\text{norm}}^{\text{opt}}$ is found by sequentially interpolating experimental $\gamma$ data onto the working surface by bilinear interpolation across the entire range of $k_{\text{norm}}$ until the 1-norm of the residuals between experimental and theoretical $N_{\text{eff}}$ values is minimized. Theoretical working surfaces were calculated for the EC$_{2X}$E reaction, and for comparison, the EC′ reaction, using the set of diffusion coefficients as defined earlier, in the range $0 \leq \gamma \leq 0.8$ and $-1.5 \leq \log(k_{\text{norm}}) \leq 1.0$.
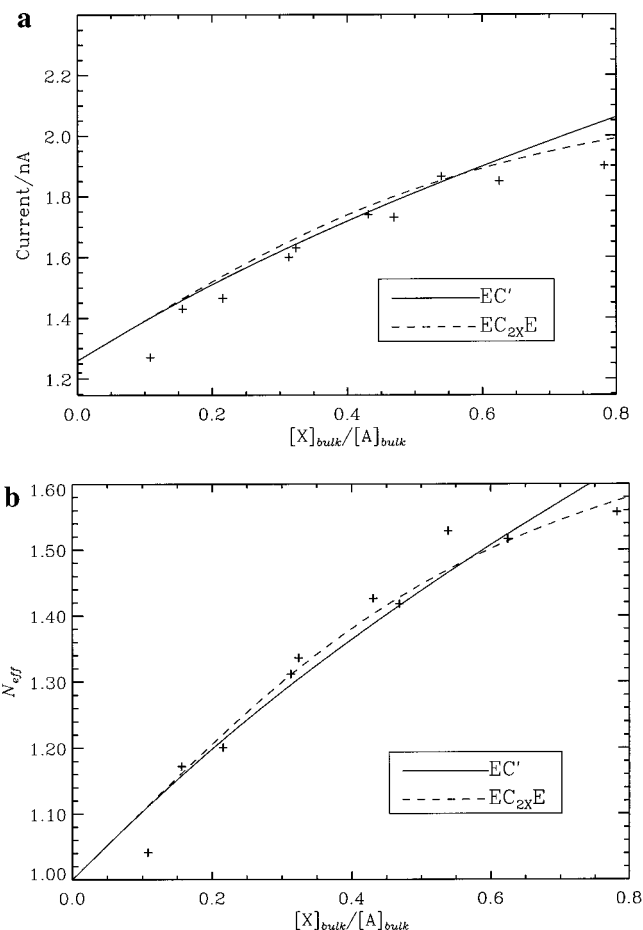


**Figure 9.** (a) Plot showing the agreement between experimentally measured current data and the theoretically calculated current at $k_{\text{norm}}^{\text{opt}}$ for the EC′ and EC$_{2X}$E reactions at the 19.5 $\mu$m microdisk electrode. (b) Plot showing the agreement between experimentally measured $N_{\text{eff}}$ data and the theoretically calculated data at $k_{\text{norm}}^{\text{opt}}$ for the EC′ and EC$_{2X}$E reactions at the 19.5 $\mu$m microdisk electrode.

Figure 9a shows experimental $N_{\text{eff}}$ data for the 19.5 $\mu$m carbon electrode plotted against $[X]_{\text{bulk}}/[A]_{\text{bulk}}$ (equivalent to $\gamma$ in the mathematical formulation of the problem) with the respective working curves for $k_{\text{norm}}^{\text{opt}}$ overlaid. As can be seen, the experimental data is modeled well by the working curves for both the EC$_{2X}$E and EC′ reactions. The fact that differences between EC$_{2X}$E and EC′ reaction working curves are much smaller than the error in the experimental data demonstrates the difficulty in differentiating these reactions by limiting current analysis.

To verify the model further, we consider the limiting current which may be analytically calculated from $N_{\text{eff}}$ using the relation

$$I = 4FCD_A r_e [A]_{\text{bulk}} N_{\text{eff}} \tag{34}$$

Plots of experimental limiting currents and theoretical working curves derived theoretically are shown in Figure 9b. The relative standard deviation between experimental results and the theoretical results for the 19.5 $\mu$m electrode is 1.9%. The fitting results in a value for $\log(k_{\text{norm}}^{\text{opt}})$ of $-0.0525$. The consistency of agreement for the working surface interpolation method is further illustrated in Figure 10, for the 7.3 and 25.0 $\mu$m platinum electrodes. The relative standard deviation between the experimental and theoretical interpolated results is 0.66% and 1.59%, respectively. The working surface interpretation results in a value of $1.4 \times 10^7$ mol$^{-1}$ cm$^3$ s$^{-1}$ (calculated as the mean of three log $k_2$ values).

Microdisk Electrode Voltammetry

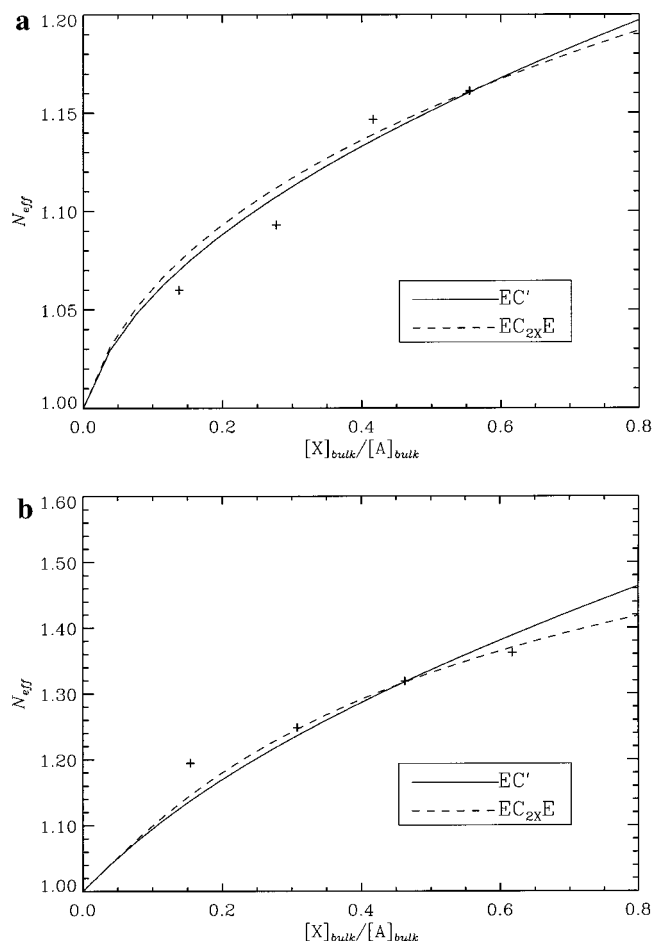*J. Phys. Chem. B, Vol. 104, No. 47, 2000* **11267**



**Figure 10.** Plots showing agreement between experimentally measured $N_{\text{eff}}$ data and the theoretically calculated data at $k_{\text{norm}}^{\text{opt}}$ for the EC′ and EC$_{2X}$E reactions at (a) 7.3 $\mu$m and (b) 25.0 $\mu$m electrodes.

## Conclusion

A general method for modeling of the EC$_{2X}$E and EC′ reaction has been illustrated. The convergence of both simulations has been considered as a consequence of the concentration distribution of the electroactive species. Furthermore, the results of the simulation of the EC$_{2X}$E reaction have been investigated using working surface interpolation of the DMPD/H$_2$S system experimental data, the reaction pathway of which has been independently verified by linear sweep and cyclic voltammetry. Working surface interpolation leads to theoretical limiting currents that are in good agreement with experimental results.

Finally, we note that the closeness of the theoretical predictions for the EC′ and EC$_{2X}$E mechanisms to the experimental data, shown in Figures 9 and 10, suggests that, unless a wide concentration range of X is experimentally accessible, the distinction between the two mechanistic pathways by steady-state microelectrode voltammetry in isolation is likely to be challenging.

## References and Notes

(1) Phillips, C. G. *J. Electroanal. Chem.* **1990**, *296*, 255.

(2) Rajendran, L.; Sangaranarayanan, M. V. *J. Electroanal. Chem.* **1996**, *415*, 1.

(3) Aoki, K.; Osteryoung, J. *J. Electroanal. Chem.* **1981**, *122*, 19.

(4) Shoup, D.; Szabo, A. J. *J. Electroanal. Chem.* **1982**, *140*, 237.

(5) Fleischmann, M.; Pletcher, D.; Denuault. *J. Electroanal. Chem.* **1989**, *263*, 225.

(6) Rajendran, L.; Sangaranarayanan, M. V. *J. Phys. Chem. B.* **1999**, *103*, 1518.

(7) Mirkin, M. V.; Bard, A. J. *J. Electroanal. Chem.* **1992**, *323*, 1.

(8) Jin, B.; Qian, W.; Bard, A. J. *J. Electroanal. Chem.* **1996**, *420*, 19.

(9) Michael, A. C.; Wightman, R. M.; Amatore, C. A. *J. Electroanal. Chem.* **1989**, *267*, 33.

(10) Taylor, G.; Girault, H. H. *J. Electroanal. Chem.* **1990**, *293*, 19.

(11) Gavaghan, D. J. *J. Electroanal. Chem.* **1989**, *456*, 1.

(12) Heinze, J. *J. Electroanal. Chem.* **1989**, *124*, 73.

(13) Heinze, J. *Ber. Bunsenges. Phys. Chem.* **1981**, *85*, 1096.

(14) Lavagini, I.; Patrore, P.; Magno, F.; Amatore, C. A. *J. Electroanal. Chem.* **1991**, *316*, 37.

(15) Alden, J. A.; Compton, R. G. *J. Phys. Chem. B.* **1997**, *101*, 8941.

(16) Alden, J. A.; Compton, R. G. *J. Phys. Chem. B.* **1997**, *101*, 9606.

(17) Amatore, C. A.; Fosset, B. *J. Electroanal. Chem.* **1992**, *328*, 21.

(18) Verbrugge, M. W.; Baker, D. R. *J. Phys. Chem.* **1992**, *96*, 4572.

(19) Ferringo, R.; Brevet, P. F.; Girault, H. H. *Electrochim. Acta* **1997**, *42*, 1895.

(20) Harriman, K.; Gavaghan, D. J.; Houston, P.; Suli, E. *Electrochem. Commun.* **2000**, *2*, 150.

(21) Nann, T.; Heinze, J. *Electrochem. Commun.* **1999**, *1*, 289.

(22) Galceran, J.; Gavaghan, D. J.; Rollett, J. S. *J. Electroanal. Chem.* **1995**, *394*, 17.

(23) Gavaghan, D. J. *J. Electroanal. Chem.* **1997**, *420*, 147.

(24) Alden, J. A.; Hutchinson, F.; Compton. R. G. *J. Phys. Chem. B* **1997**, *101*, 949.

(25) Compton, R. G.; Dryfe, R. A. W.; Wellington, R. G.; Hirst, J. *J. Electroanal. Chem.* **1995**, *383*, 13.

(26) Brandt, A. *Math. Comput.* **1977**, *31*, 333.

(27) Alden, J. A.; Compton, R. G. *J. Electroanal. Chem.* **1996**, *515*, 1.

(28) Compton, R. G.; Alden, J. A. *J. Phys. Chem. B.* **1997**, *101*, 9606.

(29) Lawrence, N. S.; Davis, J.; Jiang, L.; Jones, T. G. J.; Davies, S. N.; Compton, R.G. *Electroanalysis*, in press.

(30) Tutty, O. R. *J. Electroanal. Chem.* **1994**, *377*, 39.

(31) NAG Fortran Library Mark 18; National Algorithms Group: Oxford, UK.

(32) On a grid of $N_K = 50 \times N_J = 200$, the simulation converged a value of $N_{\text{eff}} = 1.9950$ at the kinetic limit of $k_{\text{norm}}$.

(33) Alden, J.; Compton, R. G. *J. Phys. Chem B* **1997**, *47*, 9741.

(34) Cardwell, T. J.; Mocak, J.; Santos, J. H.; Bond A. M. *Analyst* **1996**, *121*, 357.

(35) Adams, R. N. *Electrochemistry at Solid Electrodes*, Marcel Dekker: New York, 1969.

(36) Rudolph, M.; Reddy, D. P.; Feldberg, S. W. *Anal. Chem.* **1994**, *66*, 589.

(37) Contour lines are plotted at intervals of one-tenth of the maximum value of the concentration in Figures 6 and 7, or the maximum value of $K$ in Figure 5.